Two-Dimensional Ordering in Block Copolymer Monolayer Thin Films upon Selective Solvent Annealing

You Wang,* Xiaodong Hong, Baoquan Liu, Changyou Ma, and Chunfang Zhang

Materials Physics and Chemistry Department, Harbin Institute of Technology, Harbin 150001, China

Received April 3, 2008; Revised Manuscript Received May 20, 2008

ABSTRACT: The morphology evolution of poly(styrene−ethylene/butylene−styrene) monolayer thin films upon "annealing" in the vapor of cyclohexane, a selective solvent for majority poly(ethylene/butylene) block, was investigated by atomic force microscopy (AFM). The pathway information on the two-dimensional ordering from poorly ordered short cylinders, to aligned long cylinders, and then to well-ordered hexagonal spheres was revealed by repeatedly taking images of the same marked area of 2×2 μm^2 on the sample surface after ex-situ annealing treatments. It was found that the whole ordering process consists of (1) the cyclic transitions between poorly ordered cylinders and semidisordered phase via poorly ordered spheres, during which the orderliness of cylinders gradually improves, and (2) the pinching-off from enough-ordered cylinders into hex-spheres. It was noticed that part of the ordering takes place in the way of nucleation and growth, but it seems that the remaining part of ordering involves spinodal and decomposition. Post-thermal annealing results indicated the well-ordered hex-spherical structure is not in the state of thermal equilibrium. It was also observed that the ordering process slows down as the films thickness increases. Finally, it was demonstrated that this selective solvent annealing technique can be used to block copolymers at different molecular weight to tailor the size and period of monolayer hex-spherical domains.

1. Introduction

The ability of block copolymers to self-assemble into a variety of high regular domains on the 10−100 nm scale depending on the polymer species involved, the molecular weight, the average composition, and the thermotropic/lyotropic processing characteristics makes them especially suited for nanotechnical applications. Unlike any other candidate material, their nanotechnical applicability stems from not only the scale of the microdomains but also the tunability of the microdomains in shape, orderliness, orientation, size, and period afforded by changing the influential parameters mentioned above.[1–4] In the past decade, block copolymer thin films have attracted much more attention than block copolymer bulk because many new nanotechnical applications, for example fabrication of high-density arrays for data storage,[5,6] electronics,[7,8] and molecular separation,[9] are based on thin film technology. In addition, thin films involve additional variables such as film thickness and surface interactions, which could also be used for tuning block copolymer microstructure. Past studies on various ordering processes at the aim of controlling the microstructures of block copolymer thin films can be divided into two categories in terms of control item and strategy: (1) the ordering for control over shape, orderliness, and orientation by applying external fields; (2) the ordering for control over size and period by changing molecular weight or composition of block copolymers. Particular attention has been paid to the ordering for producing and/or tuning the microstructures of normal cylinders and monolayer spheres from lithographic considerations.[1–4]

1.1. Ordering for Control over Shape, Orderliness, and Orientation. Block copolymer thin films are usually prepared by spin-coating or drop-casting from solutions. The preparation process involves two competitive processes between phase separation kinetics and verification due to the evaporation of solvent. As the preparation process removes the solvent relatively quickly, regular let along equilibrium structures are not usually observed. The ordering of these structures in block

copolymer thin films is therefore the key to their successful nanotechnical applications.

Ordering Techniques. There are many recent literatures about the study on evolution, elimination of defects, and orientation of microstructures in block copolymer thin films by using various external fields, such as electrical fields,[10,11] thermal annealing,[12,13] temperature gradients,[14] shear,[15,16] graphoepitaxy,[17,18] and chemically patterned substrates.[19] In addition, solvent annealing[20–23] and solvent evaporation rate[24,25] can also be used as external fields to trigger various ordering processes. Fukunaga et al.[26,27] showed that solvent annealing can greatly enhance the ordering of copolymer morphologies in very thin films. Hahm et al.[28] and Kimura et al.[29] have also shown that the evaporation-induced flow in solvent-cast block copolymer films can produce the ordered arrays of nanoscopic cylindrical domains with a highly in-plan orientation and lateral order. Kraush and co-workers[30] reported the preparation process from solutions can lead to the formation of regular metastable structures which are induced by the selectivity of solvent.

Mechanism and Kinetics. Although a growing number of new technologies[10–29] have been developed for control over the microstructure of block copolymer thin films, little is known on the mechanism and kinetics of the ordering processes involved. From the fundamental viewpoint, a thorough and predictive understanding of the mechanism and kinetics of these ordering processes has implications for the practical control of copolymer morphology, and in turn it further enables these materials to be more suitable for nanotechnological applications. The experimental studies of the mechanism and kinetics (usually by AFM) mainly focus on the defect evolution in the highly ordered layer of cylindrical or spherical microdomains under thermal annealing conditions.[31–36] Thanks to the pioneering work of Hahm and co-workers,[31,32] the pathway information on defect evolution was revealed for the first time by ex-situ AFM imaging the same spot on the sample surface after thermal annealing treatments. It was found the evolution of cylinders takes place through relinking, joining, clustering, and annihilation. Later, in-situ AFM[33–36] was used to track the defect evolution and phase transition. Tsarkova et al.[35,36] reported the

* Corresponding author: Tel +86-451-86412516; Fax +86-451-86412516; e-mail y-wang@hit.edu.cn.
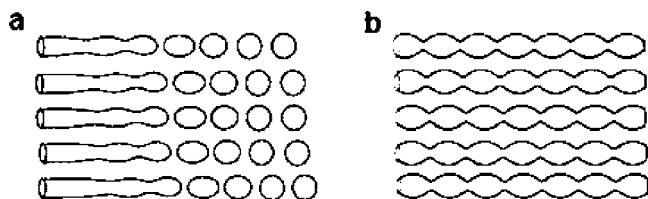
Figure 1. Schematic diagrams of transitions between cylinders and spheres through (a) nucleation and growth and (b) spinodal and decomposition.

interfacial undulations and the formation of local transitional phases, such as spheres and perforated lamella as a short-term pathway to facilitate long-term transition. Since it is difficult to simulate in theory the ordering in thin films with two kinds of complicated surface interactions of sample/superstrate (often air) and sample/substrate considered, we have to review the results drawn from block copolymer bulk. Over the past decade, theoretical studies particularly focused on the mechanism and kinetics of reversible transition between cylinders and spheres. On the basis of the time-dependent Grizburg–Landua model,[37] anisotropic fluctuation theory,[38] or self-consistent-field theory,[39] most theoretical examinations of pathways for the C ↔ S transition suggested or assumed the nucleation and growth (NG), as shown in Figure 1a. These simulation results are in good agreement with most experimental reports.[40,41] However, Ryu and Lodge reported[42,43] the existence of the C ↔ S transition via spinodal and decomposition (SD), as shown in Figure 1b, which is contrary to NG mechanism. Arguments[39] are thus aroused, and further experimental investigations are expected.

As for ordering kinetics, Tsarkova et al.[35] reported a time scale of tens of seconds for elementary steps of defect motion via interfacial undulation and repetitive transitions and inferred, according to the velocity of transition, that evolutions may take place through correlated movement of chain clusters other than diffusion transport mechanism. Harrision and co-workers[33] reported the correlation length of the nanodomains grew with the average spacing between disclinations in accordance with a power law. As a whole, both the mechanism and kinetics for a long-term large-scale ordering under many other external fields such as electric field, shear, and solvent annealing, etc., are still unknown.

Ordering Characterization. The lack of understanding on the ordering mechanism and kinetics is mainly due to the lack of efficient characterization techniques to follow the dynamic process. The ordering of microdomain in block copolymers has previously been investigated by in-situ neutron scattering[44] and small-angle X-ray scattering (SAXS),[45] of which the scattering probes look at the spatially averaged behavior only, and so they cannot provide detailed ordering pathway information. Transmission electron microscopy (TEM) or scanning electron microscopy (SEM) is limited by both the need to stain heterogeneous polymer domains for contrast enhancement and the possible irradiation damage by electron beams. Tapping-mode atomic force microscopy (TM-AFM)[31–36] has been proved so far to be the exclusive technique suitable for studying the ordering in block copolymer thin films either in situ or ex situ. Although in-situ AFM is a straightforward technique, its applicability has been limited to the tracking of thermally induced defect evolution only. Ex-situ AFM is more suitable for following most of other ordering processes caused by solvent annealing or applying electric fields, etc.; for example, the risk of exposing AFM parts to organic solvents can be avoided during in-situ solvent annealing. The following is the working strategy of ex-situ AFM: imaging a sample, treating sample ex-situ so that its morphology evolves, quenching the sample, taking another image of the same area, and so on and so forth.

Table 1. Characteristics of the Block Copolymer Materials Used for Present Study

	molecular characteristics M_n ($\times 10^{-3}$)			
designation	PS block	PEB block	M_w/M_n	PS (wt %)
SEBS G1651	29	116	1.20	32
SEBS G1650	10.3	53.3	1.19	29
SEBS G1652	7.0	37.5	1.07	32

However, performing such ex-situ imaging needs a special AFM tip relocation technique with a nanometer resolution as the scale of block copolymer microdomains are tens of nanometers. In addition, this relocation technique should not depend on the feature of the microdomain patterns of block copolymers as they can change dramatically during the ordering process. Obviously, performing such ex-situ imaging operations is not only time-consuming but also technique challenging.

1.2. Ordering for Control over Size and Period. Han et al.[46] reported the cylindrical domains with diameters ranging from 46 to 54 nm can be tuned by blending block copolymers and homopolymers and then annealing them in the solvent vapor. Russell et al.[47] reported the preparation of closely packed normal cylindrical domains with diameters ranging from 15 to 50 nm and separation distance from 24 to 89 nm by applying an external electric field to block copolymers over a board range of molecular weights. However, the tailoring of microdomain structure with this technique[47] is at the expense of losing structure orderliness for block copolymer at high molecular weight.

The present study is motivated by a previous work,[48] in which three solvents—xylene, toluene, and cyclohexane—were used to generate three different as-cast morphologies for comparing AFM with TEM data: (1) coexistence of short cylinders with branches in some cases and spheres, (2) coexistence of short cylinders without branches and spheres, and (3) spheres, respectively. We wonder whether a morphology evolution could be triggered by using one solvent casting followed by another solvent annealing. Thus, xylene, a nonselective solvent, was chosen to prepare block copolymer thin films with low surface roughness and high strength, and cyclohexane, a selective solvent for majority poly(ethylene/butylene) (PEB) block, was chosen for solvent annealing treatments expecting that such treatments will lead to the generation of spherical microdomains. Surprisingly, a long-term ordering from poorly ordered short cylinders, to aligned long cylinders, and then to well-ordered hexagonal spheres was found. With the help of a precise AFM tip relocation technique[48,49] we previously developed, pathway information in detail for the ordering process was reveled, from which an ordering mechanism was developed. The influence of film thickness on ordering kinetic behaviors was investigated as well. Finally, we demonstrated that the potential of application of this solvent annealing technique to tune the size and period of monolayer hex-spherical domains by changing the molecular weight of block copolymers, which should be of great interest for lithographic applications.

2. Experimental Section

Materials. Three asymmetric poly(styrene–ethylene/butylene–styrene) (SEBS) triblock copolymer Kraton G-1650, Kraton G-1651, and Kraton G-1652 (referred as SEBS G1650, SEBS G1651, and SEBS G1652 in this paper) were purchased from Shell Co. Their molecular weight, polydispersity, and polystyrene content are tabulated in Table 1.[50] Xylene, a nonselective solvent, and cyclohexane, a selective solvent, for PEB block are used as supplied. Alcohol in HPLC grade was purchased from TEDIA Co. Ltd. Multiwalled carbon nanotubes (MWCNTs) with diameter ranging from 10 to 30 nm were purchased from Shenzhen Nanotech Port Co., Ltd.
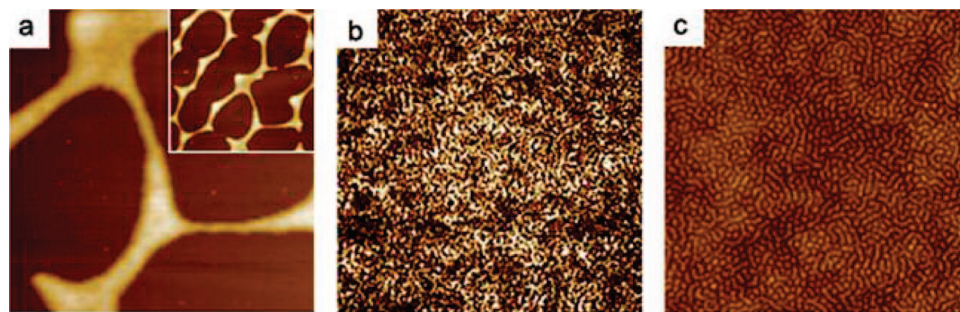
Figure 2. AFM height images of as-cast SEBS G1650 thin films with different thickness: (a) 7 nm. In the inset (right top corner), a large-scale scan of $4.0 \times 4.0 \ \mu m^2$ of the same area is shown. (b) 11 nm and (c) 16 nm. Image size: $1.5 \times 1.5 \ \mu m^2$.

Sample Preparation. The SEBS G1650 were dissolved in xylene to form solutions with three different concentrations (0.2, 0.4, and 0.8 wt %). After spin-coating each solution onto freshly cleaved mica surface at 2000 rpt for 20 s, films of 16, 28, and 44 nm thickness were produced. By increasing the spin-coating rate to 3000 rpt and keeping it for 20 s, films of 11, 20, and 35 nm thickness were prepared. Further increasing the spin-coating rate to 4000 rpt, dewetted films of about 7 nm thick was obtained from 0.2 wt % solution. Both SEBS G1651 and SEBS G1652 were also dissolved in xylene to form 0.5 wt % solution, and thin films of about 28 and 45 nm thick were prepared by spin-coating the solutions at 2000 rpm for 20 s. The thickness of films was measured by using an AFM tip scratch technique we previously developed, and the detailed description of the measurement procedure is given elsewhere.[48] For ex-situ AFM measurement, an ultrasonic cleaner was used at a frequency of about 40 kHz for ultrasonic dispersion of MWNTs. A few drops of the ultrasonic treated 0.1 wt % solution were dispersed on the as-cast SEBS G1650 film. The distribution density of carbon nanotubes was adjusted by varying the number of solution drops so that by average at least one carbon nanotube could be found in an area of $5 \times 5 \ \mu m^2$. These deposited MWNTs are used as marks for guiding the relocation of AFM tip to the same location of $2 \times 2 \ \mu m^2$. For the comparative AFM measurements, a large piece of spun-cast SEBS G1650 film (35 nm thick) on mica substrate was cut into dozens of small pieces of 0.5×0.5 cm^2 in area to enable all the samples to be measured to have the same thickness and as-cast morphology. The SEBS G1650 thin films of 0.5×0.5 cm^2 in size with different thickness are prepared in the same way for the kinetic behavior measurements.

Annealing Treatment. Solvent annealing treatment was made in a thermostatic oven at a temperature of 22 ± 0.2 °C as detailed below. A piece of filter paper was put into a Petri dish to cover the bottom. The mica substrates with the sample films on top were put on the filter paper. After adding 60 μL cyclohexane on the filter paper surrounding the samples, the dish was closely covered by putting a 500 g dead weight on top and then put the dish into the oven. By average, the filter paper remains wet for 12 h, and if necessary, an additional 60 μL of cyclohexane should be added according to the judgment of the naked eye to keep this filter paper always wet in the whole annealing process. By the way, we compared the results obtained for the annealing at 22 °C in the oven with those obtained for the annealing at ambient conditions (19 $\pm$ 2 °C), and no difference has been found. Before TM-AFM measurement, the samples were dried in a desiccator for 1−2 min. The annealing time was recorded from the moment when samples were put into or taken out from the Petri dish. For the comparative experiments, all the samples were annealed in the same Petri dish simultaneously before they were taken out for AFM measurements. Thermal annealing treatments were carried out in a vacuum oven at a temperature of 140 $\pm$ 1 °C. Liquid nitrogen gas atmosphere was used to quench the annealed sample to room temperature.

Atomic Force Microscopy. Digital Instrument multimode SPM III atomic force microscopy was performed at ambient conditions in tapping mode for imaging the topography. Without special mention, for imaging the morphology of block copolymers, the height and phase images were recorded simultaneously under

Table 2. Diameters, Periods, and Density of Hex-Spherical Domains as a Function of the Molecular Weight of Block Copolymers

block copolymer	diameter (nm)	period (nm)	sphere density
SEBSG1652	18	30	1.3×10^{11}/cm^2
SEBSG1650	23	37	8.4×10^{10}/cm^2
SEBSG1651	38	61	3.1×10^{10}/cm^2

moderate tapping conditions, with free and set point amplitudes 60 and 42 nm, respectively ($r_{sp} = 42/60 = 0.70$). During the imaging, the operating frequency was readjusted after engaging the tip on the surface such that the operating frequency was on the low-frequency side of the resonance. For the measurement of the block copolymer thin film thickness, the height image was recorded under light tapping conditions ($r_{sp} = 0.93-0.90$) to avoid the possible deformation of sample surface.[48] Commercial silicon cantilevers with spring constant ranging from 25 to 50 N m^{-1} were used. The detailed description of repeated ex-situ AFM imaging the same location on a sample surface after solvent annealing treatments is given elsewhere.[49]

3. Results and Discussion

3.1. Effect of Film Thickness on As-Cast Morphology. The as-cast morphologies of 7, 11, and 16 nm thick SEBS G1650 thin films from solutions in xylene are shown in parts a, b, and c of Figure 2, respectively. The higher domains in AFM height images and the brighter domains in AFM phase images correspond to polystyrene (PS) phase.[48] For 7 nm film, the as-cast morphology is featureless, and for 11 nm film, the microphase-separated morphology is not well-defined. Since it turned out that the solvent annealing of 7 nm films caused the dewetted films to break into pieces and the as-cast morphology of the 11 nm films does not change upon annealing in cyclohexane vapor, the microdomain ordering of thicker films ($\geq$16 nm) were investigated as detailed below. According to our experience[48,51] of studying the as-cast morphology of SEBS G1650 thin films prepared from xylene, when the thickness of the as-cast films is above 16 nm, the morphology shown in Figure 2c is representative and thickness independent. It is worthwhile to mention that given the period of the later generated hex-sphere structure of SEBS G1650 thin films is 37 nm, as shown in Table 2, special attention has been paid to the ordering in the film of 35 nm thickness, and all the sample films used for the study with thickness ranging from 16 to 44 nm are therefore considered to be monolayers.

3.2. Two-Dimensional Ordering in Block Copolymer Monolayer Thin Films. This section consists of four parts: (A) ex-situ AFM characterization of the same marked area on sample surface with hour and minute observation time intervals to obtain the ordering pathway clues; (B) comparative AFM characterization of ordering samples as a function of annealing time for comparing with ex-situ AFM data; (C) presenting an ordering mechanism on the basis of AFM data and comparing the
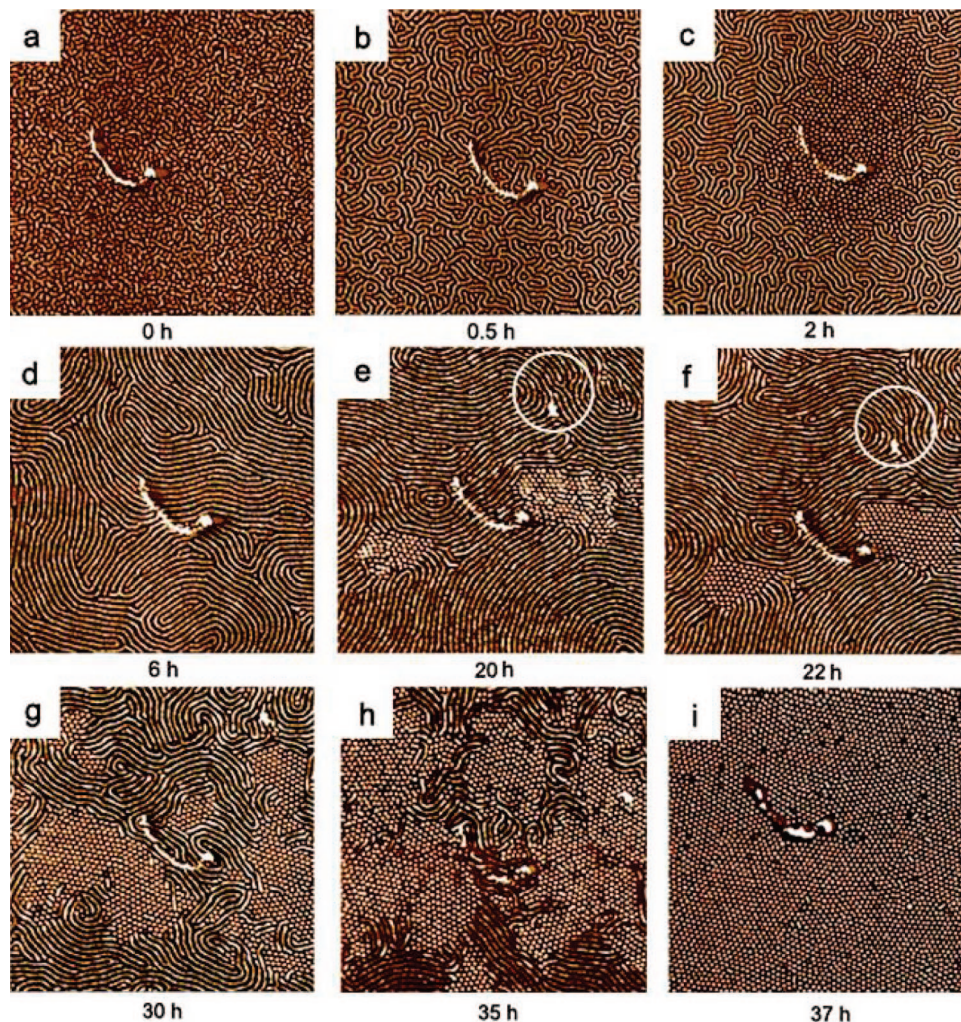
Figure 3. A set of time-lapsed AFM phase images taken consecutively from the same area of a 35 nm thick SEBS G1650 thin film after ex-situ cyclohexane vapor annealing treatments for (a) 0, (b) 0.5, (c) 2, (d) 6, (e) 20, (f) 22, (g) 30, (h) 35, and (i) 37 h. The central cylindrical feature is a carbon nanotube deposited on the sample surface as a guide for relocation of AFM tip. Image size: $2 \times 2 \ \mu m^2$.

mechanism with past results in literature; and (D) studying the influence of film thickness on the kinetic behaviors of two-dimensional ordering.

A. Ex-Situ AFM Characterization. Figures 3 and 4 each presents a set of time-lapsed AFM phase images taken consecutively from the same area ($2 \times 2 \ \mu m^2$) of a 35 nm thick SEBS G1650 thin film after repeated ex-situ cyclohexane vapor annealing treatments. Shown in Figure 3 are the images captured by using observation time interval on hour scale to have an overview of the long-term ordering process. It can be seen from these images that a microdomain ordering from poorly ordered short cylinders (Figure 3a) to highly aligned long cylinders (Figure 3d) and then to well-ordered hexagonal spheres (Figure 3i) takes place upon solvent annealing. It should be noted the reasons why we attribute the hex-spherical domains in AFM images to spherical rather than normal cylindrical structure are as follows: (1) the formation of PS spheres in either kinds of SEBS G1650 thin films cast from xylene or cyclohexane has been previously confirmed by the TEM observation[48,52] of overlapped regions between cylindrical and spherical domains or overlapped regions between spherical domains; (2) a recent study[53] suggests that spherical structure in monolayer block copolymer thin films prefers hexagonal symmetry to body-centered-cubic symmetry. By carefully comparing the time-sequenced images shown in Figure 3d–i, the pathway for the microdomain ordering from long cylinders with high orderliness to perfect hexagonal spheres via grain boundaries can be clearly

observed. First, the nucleuses of poorly ordered sphere phase as shown in Figure 3e form in the aligned long cylinder phase. Next the transformation of a poorly ordered sphere phase into a well-order hex-sphere phase then occurs (Figure 3f). Finally, the growth of hex-sphere phase encompassed the whole sample (Figure 3g–i). However, just by comparing the time-lapsed images shown in Figure 3a–d, we cannot have a clear pathway for information regarding the ordering from the initial poorly ordered short cylinders to the longer cylinders with increasing orderliness, as shown in Figure 3b,d. The only clue—the coexistence of cylinder and sphere phases (Figure 3c) after the presence of a cylinder phase with less orderliness (Figure 3b) but before the presence of a cylinder phase with high orderliness (Figure 3d)—suggests that the ordering process involved reversed transitions between cylinder and sphere phases.

In order to give a positive answer, we use a much shorter observation time interval on a minute scale to follow the initial ordering process in detail. The overall ordering time of 35 min is set to match the ordering process shown in Figure 3a, b, and the results are shown in Figure 4. It can be seen from these figures that the morphologies of cylinder phase shown in Figure 4a,k basically match those shown in Figure 3a,b regarding the improved orderliness of cylinder phase. To our surprise, three consecutive transition cycles were observed as shown in Figure 4a–d, Figure 4d–h, and Figure 4h–k, respectively. In each cycle, the microdomain ordering proceeds from poorly ordered cylinders, to poorly ordered spheres, to semidisordered
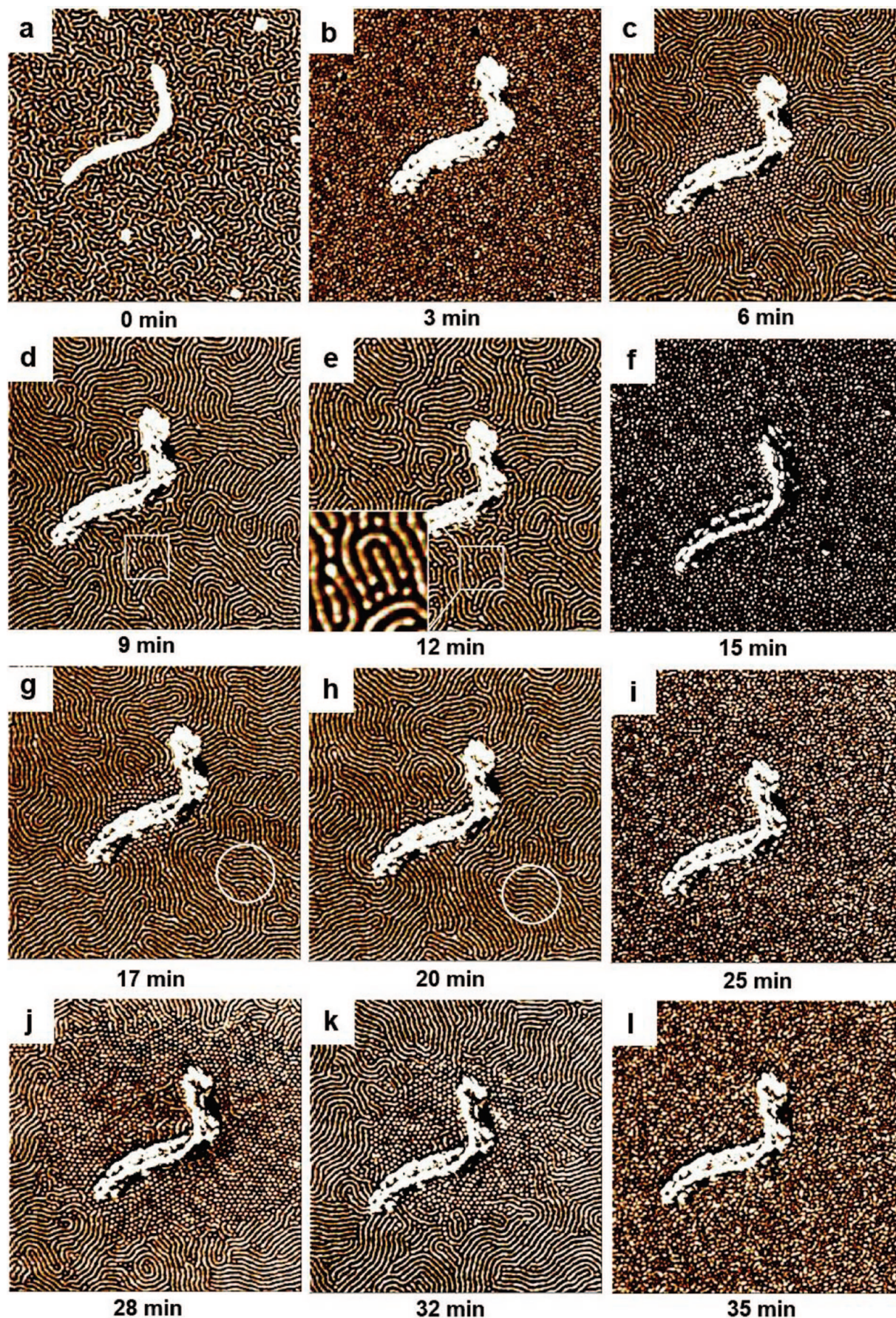
Figure 4. A set of time-lapsed AFM phase images taken consecutively from the same area of a 35 nm thick SEBS G1650 thin film after ex-situ cyclohexane vapor annealing treatments for (a) 0, (b) 3, (c) 6, (d) 9, (e) 12, (f) 15, (g) 17, (h) 20, (i) 25, (j) 28, (k) 32, and (l) 35 min. The central cylindrical feature is a carbon nanotube deposited on the sample surface as a guide for relocation of AFM tip. Image size: 2×2 μm^2.
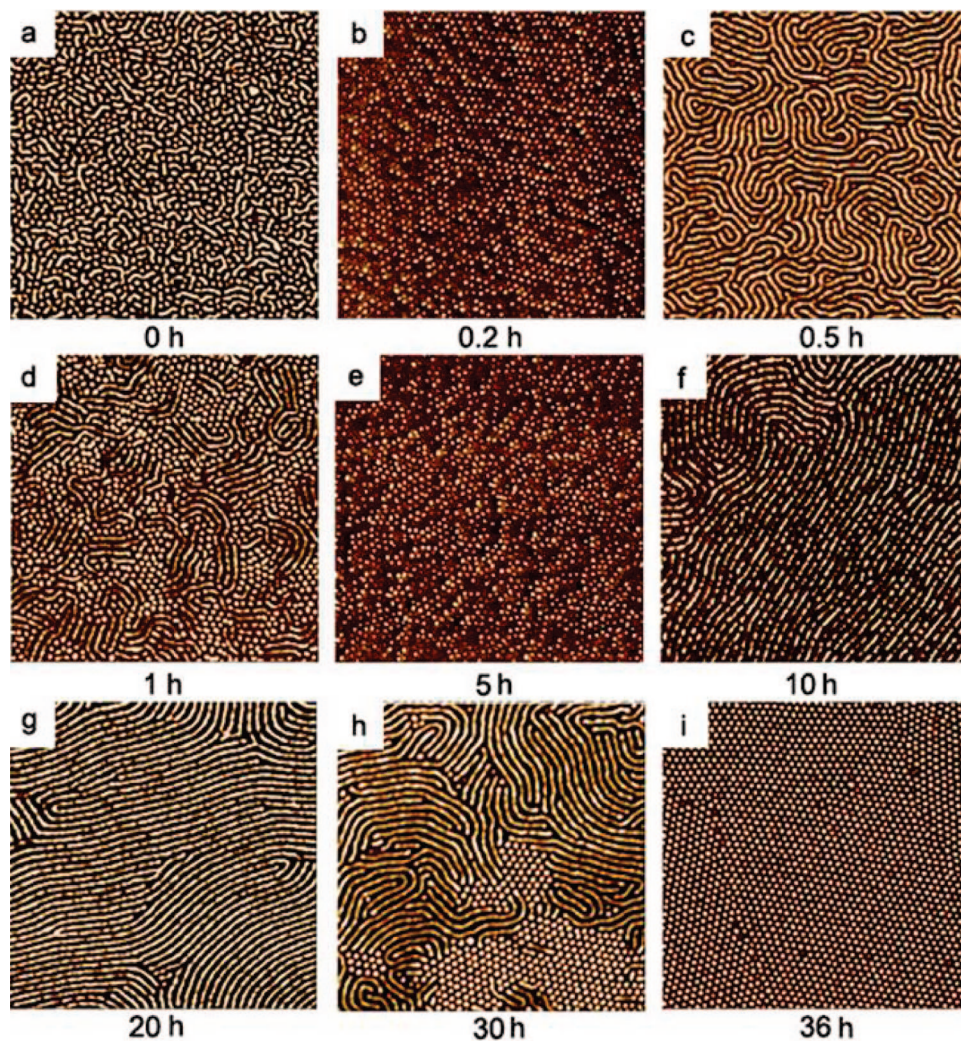
Figure 5. AFM phase images of 35 nm thick SEBS G1650 thin films after annealing in cyclohexane vapor for (a) 0, (b) 0.2, (c) 0.5, (d) 1, (e) 5, (f) 10, (g) 20, (h) 30, and (i) 36 h. Image size: $2 \times 2 \ \mu m^2$.

phase, to poorly ordered spheres, and then back to cylinders with improved orderliness (see Figure 4d−h for the whole process). It should be noted that although Figure 4k did not show a complete cylinder phase, the existence of such a state between Figure 4k,l can be justified by comparing Figure 4j−l. Here, the reasons why we call the images shown in Figure 4b,f,i,l semidisordered phase rather than poorly ordered spheres are (1) the average 15 nm domain size of the semidisordered phase is much smaller than the 20 nm average diameters of poorly ordered spheres, (2) the semidisordered phase is not a well-defined microphase-separated structure with blurred boundaries, and (3) the AFM phase images of semidisordered phase show an unusual dark color (Figure 4b,f). Further discussion on the semidisordered phase will be given later. It is worthwhile to mention that the simultaneously captured AFM height images always show an intact film surface without any terrace or hole. It can be seen from the careful examination of the pathway of transitions that half of the cyclic transition process from semidisordered phase, to spheres, and then to cylinders (see Figure 4b−d and Figure 4f−h) involves the nucleation and growth mechanism. However, for the other half-cyclic transition process from cylinders, to spheres, and then to the semidisordered phase (Figure 4d−f), the fluctuation of cylinders across the sample surface is observed as shown in the squared area of Figure 4e, and thus SD mechanism is assumed. During imaging the cyclic transitions shown in Figure 4 as well as many others, we found it is very difficult to capture an intermediate stage

for the cylinder to semidisordered phase transition. The different kinetic behavior observed in this part of transition process seems to further support our assumed SD mechanism.

The local-scale defect evolution through dislocation, relinking, and annihilation has also been frequently observed as shown in the circled area of Figure 3e,f and of Figure 4g,h. However, since it has been well documented recently in the literature,[31–33,35,36] on the one hand, and it does not play a key role in the ordering process as we observed, on the other, we would like not to go into too much detail. Up to now, it seems that the question concerning the pathway for transforming poorly ordered cylinders into cylinders with long-range order has been answered.

B. Comparative AFM Characterization. One may argue, however, that the transition cycles you observed may be due to the repeated cycles of annealing for ex-situ AFM characterizations, during which the original ordering process is interrupted. With the possible argument in mind, we perform a comparative AFM characterization as a function of annealing time in order to make a further comparison with ex-situ AFM data. Figure 5 shows a set of AFM phase images of 35 nm thick SEBS G1650 thin films after they are annealed in cyclohexane vapor for different periods of time. By comparing these images from a dynamic point of view with the knowledge established in the previous ex-situ AFM characterizations, the same pathway as we presented earlier can be judged on the basis of the following facts: (1) As the annealing time increases, longer cylinders with
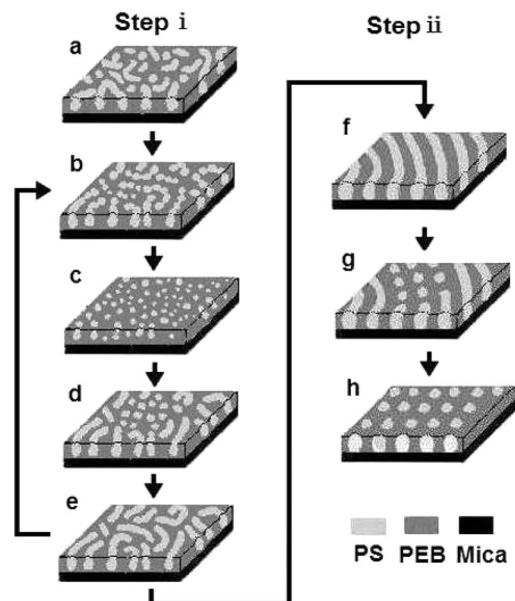
Figure 6. Schematic representation of two-step microdomain ordering in block copolymer monolayer thin films upon cyclohexane vapor annealing: (i) cyclic transitions from (a) cylinders, to (b) poorly ordered spheres, to (c) semidisordered phase, to (d) poorly ordered spheres, and then back to (e) cylinders with higher order degree, during which the orderliness of newly generated cylinders gradually increase; (ii) a pinching-off from (f) the enough-ordered cylinders into (g, h) well-ordered hex-spheres along cylindrical axes.

a gradually increased orderliness (Figure 5c,g) was observed, and a well-ordered hex-sphere structure (Figure 5i) was generated in the end. (2) In the ordering process, the semidisordered phase (Figure 5b,e) and coexistence of cylinders and spheres (Figure 5d,h) can be observed repeatedly. (3) The fluctuation-induced cylinder-to-sphere transition shown in Figure 5f is supportive of our assumption on spinodal pathway. In general, the information shown in Figure 5 coincides well with those shown in Figures 3 and 4.

C. Mechanism. On the basis of the ex-situ and comparative AFM results, we present a schematic diagram in Figure 6 in which the pathway for the ordering from poorly ordered short cylinders, to highly aligned long cylinders, and then to well-ordered hexagonal spheres is given. The complex microdomain ordering process consists of two steps: (i) the cyclic transitions from (a) poorly ordered cylinders, to (b) poorly ordered spheres, to (c) semidisordered phase, to (d) poorly ordered spheres, and then back to (e) cylinders with higher orderliness again (Figure 6a–e); (ii) the pinching-off from highly aligned cylinders into hex-spheres (Figure 6f–h). Part of the cyclic transitions in step i as shown in Figure 6a–c proceeds through SD. The remaining part of the transitions in step i (Figure 6c–e) and in step ii (Figure 6f–h) proceeds through NG.

In the following discussion, we compared this ordering mechanism with past experimental and theoretical results. We start our discussion with the three characteristics of the ordering mechanism: (1) NG and SD, (2) pathway for the cyclic transitions, and (3) the semidisordered phase. For NG, our AFM data demonstrated the NG conclusion drawn from block copolymer bulk in previous literature is also applicable to block copolymer thin films. For SD, Ryu and Lodge[42,43] reported the observation of spinodal C ↔ S transitions in block copolymer bulk triggered by the fluctuation of cylinders. They also pointed out that the energy barrier to the growth of fluctuation, which was probably due to the space mismatch between cylinder and sphere phases can cause the existence of fluctuating and nonfluctuating regions. Thus, the coexistence of cylinders and spheres shown in squared area of Figure 4e may not necessarily

lead to the conclusion that the transition from poorly ordered cylinders to spheres proceeds through NG. On the contrary, the observation of the separated spheres distributed evenly across the captured image (Figure 4e), the fluctuation of cylinders (see inset of Figure 4e), and the dynamic behaviors different from NG indicates this part of the cyclic transitions involves a spinodal mechanism. A similar fluctuation induced cylinder-to-sphere transition in block copolymer thin films has been reported by Jahm et al.[31] Here, we guess the remaining power of the fluctuation after the cylinder-to-sphere transition further leads to the following sphere to semidisordered phase transition. However, one may ask the reason why in the presented mechanism the cylinder-to-sphere transition proceeds through SD in step i and through NG in step ii. Our tentative explanation is that we found that during the solvent annealing process the average diameter of cylinders increases from the initial 14 nm (Figure 3a) to final 19 nm (Figure 3e). Such an increase makes the later generated cylinders so strong that the fluctuation could not break them into pieces. Thus, the cylinder-to-sphere transition has to proceed through NG in step ii.

As far as the pathway for the cyclic transitions, Bates et al.[54] reported their observations of transient sphere structure during the melting of cylinders in shear-cessation experiments. Qi and Wang[37] confirmed that according to the time-dependent Landau–Ginzburg calculation, if a temperature jumps slightly into the disordered phase, the melting of cylinder phase goes through a transient sphere phase. Their transition pathway from cylinders to disordered phase via spheres is basically consistent with what is shown in Figure 6a–c for half of the transition cycle. Previously, we studied the influence of casting temperature on morphology of SEBS G1650 thin films.[52] On the basis of the TEM observation of sphere phase surrounding cylinder phase within a disordered phase for samples cast at 100 °C, we inferred the existence of such a transitional pathway that sphere phase first nucleated in the disordered phase and then transformed into the cylinder phase through NG. This result is much like the pathway for the other half of the transition cycle as shown in Figure 6c–e.

As for the observed semidisordered phase, Krishnamoorti et al.[55] reported that morphology transition from short cylinders to hex-spheres possibly via a mesoscopically poorly ordered phase (an excited state). By comparing their TEM data shown in Figure 3 of ref 55 with our AFM data, we strongly believe that what they called "mesoscopically poorly ordered phase" is in fact what we called semidisordered phase because these images share two distinct characteristics in common: (1) domain size much smaller than the average diameter of spheres and (2) not well-defined microphase-separated structure with boundaries blurred. In addition, most of the captured AFM phase images of the semidisordered phases show an unusual dark color, suggesting a low modulus characteristic associated with the structure, which is consistent with the dynamic isothermal frequency scan measurements,[55] suggesting the structure has liquidlike flow characteristics. Tsarkova and co-workers[35,36] recently reported that morphology transitions may proceed via some excited states, and a cooperative movement of cluster of chains rather than the previously believed molecular diffusion can be the dominant transport process. If so, the semidisordered phase can be explained as a mixture at chain-cluster level in contrast to the fact that disordered phase is a mixture at a single chain level. By forming the semidisordered phase instead of the disordered phase, a much lower free energy barrier has to be overcome in the transition process. However, we could not completely rule out the possibility of the formation of a transient disordered phase, which can be too difficult to be a "snapshot".

Now, we are trying to make a tentative discussion regarding the driving force for the solvent annealing induced ordering to

explain the puzzling cyclic transitions observed during our experiment. It is well-known that the ordering of block copolymers is driven by total free energy minimization, with enthalpic and entropic contributions. For a given structure, e.g. either a cylinder or sphere, it is easy to understand from the enthalpic consideration that the higher the orderliness formed by a structure, the lower the free energy level a system has. Specifically in our case, selective cyclohexane preferentially swells the rubber matrix and thus increases the effective volume fraction of the rubber component. For the asymmetrically solvent swollen block copolymer system, the well-ordered hex-spheres with lowest free energy is more favorable than the long-range order cylinders when the free energy associated with conformation entropy plays a dominant role on the microdomain formation, let alone the as-cast poorly ordered cylinders. Thus, there is a strong tendency for structure transition from poorly ordered cylinders to well-ordered hex-spheres to take place in this system. On first sight, a straightforward transition pathway should be a direct cylinder-to-hex-sphere transition. For cylinders with long-range order, such a direction transition[41–43] has been well documented in bulk samples. However, for poorly aligned short cylinders like our case, the direct pinching-off from cylinders into spheres can be hampered due to the mismatch in domain orientation and domain spacing between the two phases, and the previous study[55] indicated the semidisordered phase was generated as an intermediate state to enable the transition to take place. Our on-going study suggests this transition pathway does exist but it is only found for the sample film of 16 nm thickness. The detailed results will be reported later. For the films with thickness ranging from 20 to 44 nm, for some reason which cannot be explained at present, the transition undergoes multiple intermediate states as represented by different cylinder phases with improved orderliness. Note the increase in the orderliness of parallel cylinders upon thermal and solvent annealing has been well documented in the literature,[12,13,45,49] and we demonstrated the two-dimensional transition from one cylinder phase with low orderliness to another cylinder phase with improved orderliness is mediated by the semidisordered phase. Given the fact that the sphere phase lies in between the cylinder phase and the disordered phase in the equilibrium phase diagram, the observed pathway (cylinders, to spheres, to semidisordered phase, to sphere, and then back to cylinders) as shown in step i of Figure 6 for each transition cycle can be justified. By repeating many of such transition cycles, the free energy is lowered step-by-step until an enough-ordered cylinder phase with a period of 34 nm is generated. By forming the cylinders with long-range order, the match degree of domain orientation and domain spacing is improved. So, the well-ordered hex-spheres of 37 nm in period can be generated via a direct cylinder-to-sphere transition (see step ii of Figure 6) to lower the free energy of the system to the lowest level. Following this line of thought, we further deduce the well-ordered hex-sphere structure is stable only in the presence of cyclohexane. Although, it can be preserved in the absence of cyclohexane as observed due to verification effect, the structure should belong to a nonequilibrium state. Vacuum-annealing the samples with the well-ordered hex-sphere structure confirms our deduction. After thermal annealing at 140 °C for 1 h, part of hex-spheres has coalesced into cylinders as shown in Figure 7. This result is consistent with our previous study[48] on thermal annealing of SEBS G1650 thin films.

Next, we turn our discussion to the mechanism for two-dimensional ordering of cylinders parallel to the film surface under either thermal annealing or solvent annealing conditions. Previously, an in-situ AFM study[33] suggested that defect evolution is the dominant route for the long-range order of block copolymers. However, all the in-situ and ex-situ AFM re-
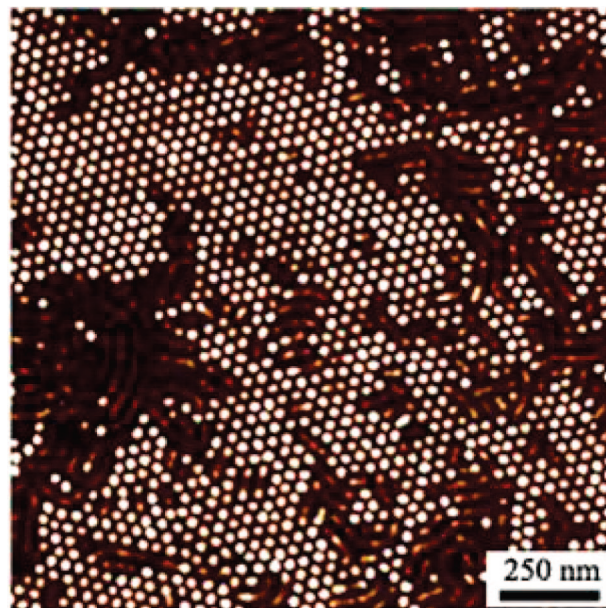

Figure 7. AFM phase image of SEBS G1650 thin film sample with hex-sphere structure after post-thermal annealing at 140 °C for 1 h.
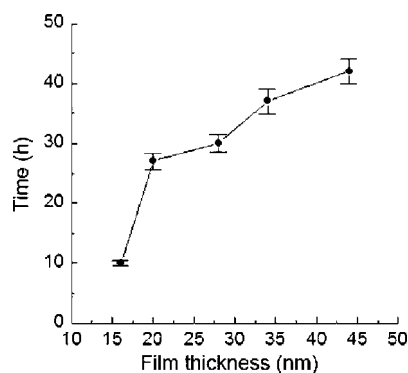

Figure 8. Influence of block copolymer film thickness on total two-dimensional ordering time for transition from poorly ordered short cylinders to well-ordered hexagonal spheres.

sults[31–36] presented so far have been limited to local-scale and short-term imaging which does not cover the whole ordering process, for example, the transition from an initial poorly ordered wormlike cylinders to a later highly orientated cylinders. In our case, the experimental results based on tracking a large scale (across the entire sample), long-term (covering whole process), and full evolution degree (from poorly ordered to well-ordered states) ordering process suggest the cyclic transitions between different phases rather than the accompanying defect evolution are the main route.

Finally, we would like to make an extended discussion on the mechanism of three-dimensional transition from parallel to normal cylinders based on our observed results of two-dimensional cylinder-to-sphere transition. Previously, Russell et al.[56] reported a two-step mechanism for the transition from parallel to normal cylinders under an electric field: (1) the original parallel cylinders fluctuate and break apart into spheres first; (2) these spheres gradually elongate and coalesce into cylinders again with the perpendicular orientation later. After a careful review of AFM and TEM results regarding the transitions between parallel cylinders and normal ones, we found the images shown in Figure 1 of refs 21, 24, and 25 and Figure 4 of ref 45 show the projections of coexistence of normal and
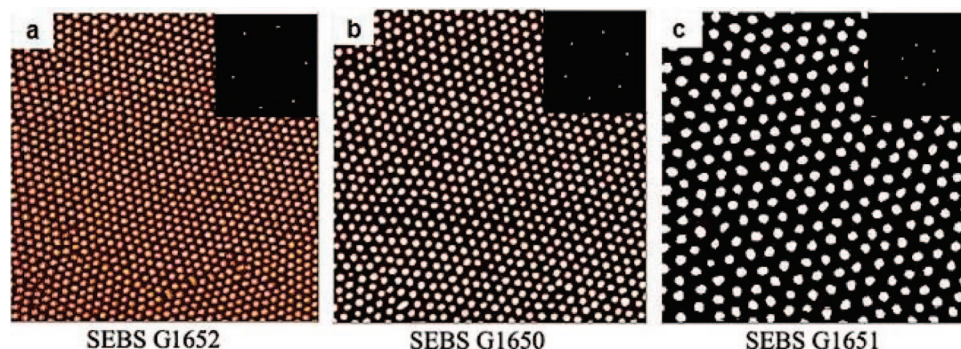
Figure 9. AFM phase images of monolayer SEBS thin films with hex-sphere structure as a function of different molecular weight: (a) 51K, (b) 74K, and (c) 174K after cyclohexane vapor annealing for 45, 37, and 55 h, respectively. The fast Fourier transform pattern in the insets proves perfected hexagonal arrays. Image size: $1.0 \times 1.0 \ \mu m^2$.

parallel cylinders are surprisingly like the two-dimensional ongoing pinching-off from cylinders into spheres at the grain boundaries (see Figure 3h). This similarity plus the established knowledge on the two-dimensional transition inspired us to speculate that this mechanism might have a universal meaning for transitions from parallel to normal cylinders because from a dynamic point of view, the observed spherical domains at the grain boundary between parallel and "normal" cylinders might be at beginning the epitaxially pinched-off spheres as we observed in Figure 3h according to step 1 of the mechanism and later the coalesced normal cylinders according to step 2 of the mechanism.

As far as we know, this work may be the first to show the ordering in block copolymer thin films could proceed via cyclic transitions between different phases. The result indicates two-dimensional ordering in thin films is much more complex than anticipated so far[35,36] and quite different from the three-dimensional ordering investigated in bulk. Because of this complicity, the arguments we give here are by no means conclusive, let alone the speculations. One of our main purposes for this discussion is to shed as much light as possible on this little-known but fundamentally important research area.

D. Kinetic Behaviors. We now turn from the mechanism to the kinetic behaviors of two-dimensional ordering in block copolymer monolayer thin films. Figure 8 shows the ordering time for the transition from poorly ordered short cylinders to well-ordered hexagonal spheres as a function of film thickness. It can be seen from Figure 8 that the ordering process speeds up as indicated by the decreasing ordering time as the film thickness decreases. We noticed this result seems to be contradictory to the previous one drawn from the 7 and 11 nm sample films. As mentioned earlier, for 11 nm films, the ordering in microphase-separated morphology is difficult, and for 7 nm films even microphase separation process becomes difficult. The contradictory changing trends observed for thick (>16 nm) and thin films enabled us to assume the existence of a critical vale for film thickness, which separates the dynamic ordering behaviors in block copolymer thin films as a result of the interplay of geometric confinement and surface field.[57] Below the critical value when film thickness is much less than microdomain period, the geometric confinement plays a dominant role, and thus the development of microdomain ordering is impeded by preventing chains from moving. Above the critical value, the preferential attraction of PEB block to the surface[48] (the surface field) plays a dominant role and induces the additional rearrangement of microdomains near the surface in favor of the microdomain ordering. The power of surface field is strong for very thin films as the effect of both surfaces combines, and it decays rapidly for thicker films. Thus, a higher film thickness leads to a lower ordering rate. Even though our

discussions on ordering behaviors are still rather descriptive at present, we felt that they might represent a step forward in the understanding the influence of sample geometry on ordering kinetics.

3.3. Tuning Size and Period of Monolayer Hex-Spherical Domains. Having studied the mechanism and kinetics of microdomain ordering, we now focus on the possibility of tuning the size and period of well-ordered hex-spherical domains by introducing SEBS G1651 and G1652 with molecular weight different from that of SEBS G1650. The monolayer thin films of the three block copolymers were prepared with thickness close to the periods of the generated spherical domains. The as-cast morphologies of SEBS G1651 and G1652 thin films are much like that of SEBS G1650 as shown in Figure 2c, except for the size and period of cylindrical microdomains (AFM results not shown). It can be seen in Figure 9 that the poorly ordered short cylinders have transformed into well-ordered hexagonal spheres as confirmed by the fast Fourier transform (FFT) patterns in the insets for all the three copolymers after cyclohexane vapor annealing for 45, 37, and 55 h. The three images show an increase in both size and period of hex-spherical domains with increased molecular weight of block copolymer. To be more specific, the diameters of spherical domains increases from 18 to 38 nm with the lattice period varying form 30 to 61 nm, as shown in Table 2. It should be noted that the AFM data of the diameters of the spherical domains can be somewhat enlarged due to AFM tip shape effect[48,58] while the measured lattice period should be correct. It can be seen from Figure 9c that the perfect hex-spherical patterns are independent of the molecular weight even at 170K levels, which mean there is still some room for a further increase in the size of a hex-spherical structure. We believe the use of very simple and cost-efficient solvent annealing technique to produce and tune well-ordered monolayer spherical structures on the tens of nanometers scale can make this kind of material a promising candidate for creation of nanostructures.

4. Conclusions

The pathway information regarding a long-term and large-scale two-dimensional ordering from wormlike short cylinders, to highly aligned long cylinders, and then to well-ordered hexagonal spheres in triblock copolymer monolayer thin films was revealed in this paper for first time by ex-situ AFM. The whole ordering process consists of (i) the cyclic transitions between cylinders and semidisordered phase mediated by poorly ordered spheres, during which the orderliness of cylinders gradually improves, and (ii) pinching-off from enough-ordered cylinders into well-ordered hex-spheres along cylindrical axes. It was noticed that part of the transition proceeds through nucleation and growth and the remaining part

seems to involve spinodal and decomposition. Our results also suggest that the cyclic transitions between different phases rather than the accompanying defect evolution are the main route for improving the alignment of cylinders parallel to the film surface. Post-thermal annealing results indicate the well-ordered hex-spheres is not in the state of thermal equilibrium but a metastable state induced by the selectivity of the solvent. The film thickness was found to have a significant influence on the ordering kinetics. The as-cast morphology of the 11 nm thick film does not change upon annealing, while increasing the film thickness (>16 nm) slows down the microdomain ordering process. In addition, the potential application of this solvent annealing technique to block copolymers at different molecular weight for tailoring diameters of the well-ordered monolayer spherical microdomains from 18 to 38 nm and period from 30 to 61 nm has been demonstrated. This comprehensive control over the shape, orderliness, size, and period of spherical microdomains in monolayer block copolymer thin films by the selective solvent annealing technique should be of great interest for lithographic applications, e.g., as template for production of quantum dot arrays.

References and Notes

(1) Park, C.; Yoon, J.; Thomas, E. L. *Polymer* **2003**, *44*, 6725.
(2) Darling, S. B. *Prog. Polym. Sci.* **2007**, *32*, 1152.
(3) Hamley, I. W. *Nanotechnology* **2003**, *14*, R39.
(4) Segalman, R. A. *Mater. Sci. Eng., R* **2005**, *48*, 191.
(5) Park, M.; Harrison, C.; Chaikin, P. M.; Register, R. A.; Adamson, D. H. *Science* **1997**, *276*, 1401.
(6) Thurn-Albrecht, T.; Steiner, R.; DeRouchey, J.; Stafford, C. M.; Huang, E.; Bal, M.; Tuominen, M.; Hawker, C. J.; Russell, T. *Adv. Mater.* **2000**, *12*, 787.
(7) Black, C. T.; Guarini, K. W.; Milkove, K. R.; Baker, S. M.; Russell, T. P.; Tuominen, M. T. *Appl. Phys. Lett.* **2001**, *79*, 409.
(8) Aswal, D. K.; Lenfant, S.; Guerin, D.; Yakhmi, J. V.; Vuillaume, D. *Anal. Chim. Acta* **2006**, *568*, 84.
(9) Zhao, D.; Feng, J.; Huo, Q.; Melosh, N.; Fredrickson, G. H.; Chmelka, B. F.; Stucky, G. D. *Science* **1998**, *279*, 548.
(10) Thurn-Albrecht, T.; Schotter, J.; Kastle, C. A.; Emley, N.; Shibauchi, T.; Krusin-Elbaum, L.; Guarini, K.; Black, C. T.; Tuominen, M. T.; Russell, T. P. *Science* **2000**, *290*, 2126.
(11) Xu, T.; Zvelindovsky, A. V.; Sevink, G. J. A.; Gang, O.; Ocko, B.; Zhu, Y. Q.; Gido, S. P.; Russell, T. P. *Macromolecules* **2004**, *37*, 6980.
(12) van den Berg, R.; de Groot, H.; van Dijk, M. A.; Denley, D. R. *Polymer* **1994**, *35*, 5778.
(13) Motomatsu, M.; Mizutani, W.; Tokumoto, H. *Polymer* **1997**, *38*, 1779.
(14) Bodycomb, J.; Funaki, Y.; Kimishima, K.; Hashimoto, T. *Macromolecules* **1999**, *32*, 2075.
(15) Albalak, R. J.; Capel, M. S.; Thomas, E. L. *Polymer* **1998**, *39*, 1647.
(16) Villar, M. A.; Rueda, D. R.; Ania, F.; Thomas, E. L. *Polymer* **2002**, *43*, 5139.
(17) Segalman, R. A.; Yokoyama, H.; Kramer, E. J. *Adv. Mater.* **2001**, *13*, 1152.
(18) Cheng, J. Y.; Ross, C. A.; Thomas, E. L.; Smith, H. I.; Vancso, G. J. *Appl. Phys. Lett.* **2002**, *81*, 3657.
(19) Rockford, L.; Mochrie, S. G. J.; Russell, T. P. *Macromolecules* **2001**, *34*, 1487.
(20) Cavicchi, K. A.; Berthiaume, K. J.; Russell, T. P. *Polymer* **2005**, *46*, 11635.
(21) Xuan, Y.; Peng, J.; Cui, L.; Wang, H. F.; Li, B. Y.; Han, Y. C. *Macromolecules* **2004**, *37*, 7301.
(22) Zhao, J. C.; Jiang, S. C.; Ji, X. L.; An, L. J.; Jiang, B. Z. *Polymer* **2005**, *46*, 6513.
(23) Niu, S. J.; Saraf, R. F. *Macromolecules* **2003**, *36*, 2428.
(24) Kim, G.; Libera, M. *Macromolecules* **1998**, *31*, 2569.
(25) Kim, G.; Libera, M. *Macromolecules* **1998**, *31*, 2670.
(26) Fukunaga, K.; Elbs, H.; Magerle, R.; Krausch, G. *Macromolecules* **2000**, *33*, 947.
(27) Fukunaga, K.; Hashimoto, T.; Elbs, H.; Krausch, G. *Macromolecules* **2002**, *35*, 4406.
(28) Hahm, J.; Sibener, S. J. *Langmuir* **2000**, *16*, 4766.
(29) Kimura, M.; Misner, M. J.; Xu, T.; Kim, S. H.; Russell, T. P. *Langmuir* **2003**, *19*, 9910.
(30) Elbs, H.; Drummer, C.; Abetz, V.; Krausch, G. *Macromolecules* **2002**, *35*, 5570.
(31) Hahm, J.; Sibener, S. J. *J. Chem. Phys.* **2001**, *114*, 4730.
(32) Hahm, J.; Lopes, W. A.; Jaeger, H. M.; Sibener, S. J. *J. Chem. Phys.* **1998**, *109*, 10111.
(33) Harrison, C.; Adamson, D. H.; Cheng, Z. D.; Sebastian, J. M.; Sethuraman, S.; Huse, D. A.; Register, R. A.; Chaikin, P. M. *Science* **2000**, *290*, 1558.
(34) Knoll, A.; Lyakhova, K. S.; Horvat, A.; Krausch, G.; Sevink, G. J. A.; Zvelindovsky, A. V.; Magerle, R. *Nat. Mater.* **2004**, *3*, 886.
(35) Tsarkova, L.; Knoll, A.; Magerle, R. *Nano Lett.* **2006**, *6*, 1574.
(36) Tsarkova, L.; Horvat, A.; Krausch, G.; Zvelindovsky, A. V.; Sevink, G. J. A.; Magerle, R. *Langmuir* **2006**, *22*, 8089.
(37) Qi, S. Y.; Wang, Z. G. *Phys. Rev. Lett.* **1996**, *76*, 1679.
(38) Laradji, M.; Shi, A. C.; Noolandi, J.; Desai, R. C. *Macromolecules* **1997**, *30*, 3242.
(39) Matsen, M. W. *J. Chem. Phys.* **2001**, *114*, 8165.
(40) Sakurai, S.; Hashimoto, T.; Fetters, L. J. *Macromolecules* **1996**, *29*, 740.
(41) Sakurai, S.; Kawada, H.; Hashimoto, T.; Fetters, L. J. *Macromolecules* **1993**, *26*, 5796.
(42) Ryu, C. Y.; Vigild, M. E.; Lodge, T. P. *Phys. Rev. Lett.* **1998**, *81*, 5354.
(43) Ryu, C. Y.; Lodge, T. P. *Macromolecules* **1999**, *32*, 7190.
(44) Krishnamoorti, R.; Silva, A. S.; Modi, M. A.; Hammouda, B. *Macromolecules* **2000**, *33*, 3803.
(45) Cavicchi, K. A.; Russell, T. P. *Macromolecules* **2007**, *40*, 1181.
(46) Peng, J.; Gao, X.; Wei, Y. H.; Wang, H. F.; Li, B. Y.; Han, Y. C. *J. Chem. Phys.* **2005**, *122*, 114706.
(47) Xu, T.; Kim, H. C.; DeRouchey, J.; Seney, C.; Levesque, C.; Martin, P.; Stafford, C. M.; Russell, T. P. *Polymer* **2001**, *42*, 9091.
(48) Wang, Y.; Song, R.; Li, Y. S.; Shen, J. S. *Surf. Sci.* **2003**, *530*, 136.
(49) Cao, Y. Z.; Liang, Y. C.; Dong, S.; Wang, Y. *Ultramicroscopy* **2005**, *103*, 103.
(50) Chen, B.; Li, X. L.; Xu, S. Q.; Tang, T.; Zhou, B. L.; Huang, B. T. *Polymer* **2002**, *43*, 953.
(51) Cao, Y. Z.; Wang, Y.; Xing, Y. M.; Dong, S. *Polym. Prepr.* **2003**, *44*, 901.
(52) Wang, Y.; Shen, J. S.; Long, C. F. *Polymer* **2001**, *42*, 8443.
(53) Stein, G. E.; Kramer, E. J.; Li, X. F.; Wang, J. *Macromolecules* **2007**, *40*, 2453.
(54) Bates, F. S.; Koppi, K. A.; Tirrell, M.; Almdal, K.; Mortensen, K. *Macromolecules* **1994**, *27*, 5934.
(55) Krishnamoorti, R.; Modi, M. A.; Tse, M. F.; Wang, H. C. *Macromolecules* **2000**, *33*, 3810.
(56) Xu, T.; Zvelindovsky, A. V.; Sevink, G. J. A.; Lyakhova, K. S.; Jinnai, H.; Russell, T. P. *Macromolecules* **2005**, *38*, 10788.
(57) Knoll, A.; Horvat, A.; Lyakhova, K. S.; Krausch, G.; Sevink, G. J. A.; Zvelindovsky, A. V.; Magerle, R. *Phys. Rev. Lett.* **2002**, *89*, 035501.
(58) Wang, Y.; Chen, X. Y. *Ultramicroscopy* **2007**, *107*, 293.